(Received 1 October 2025, Accepted 10 December 2025, Scheduled 12 January 2026)

Bandwidth Reconfigurable Circularly Polarized Antenna with Beam Steering Ability Using Phase Gradient Metasurface

Naveen Jacob[1,*], Muralidhar Kulkarni[2], and Krishnamoorthy Kandasamy[2]

[1]*Department of Electronics & Communication Engineering, Viswajyothi College of Engineering & Technology Vazhakulam, Kerala, India*
[2]*Department of Electronics & Communication Engineering, National Institute of Technology Karnataka Surathkal, Mangalore, India*

ABSTRACT: A bandwidth tunable, circularly polarized (CP) patch antenna, with a complementary split ring resonator (CSRR), embedded on the ground plane is presented in this paper. The antenna is capable of switching between ultra-wideband (UWB) frequency response, spanning through 2.6 GHz to 12 GHz, and a narrowband (NB) frequency response at 6 GHz. The excitation of CSRR results in negative permittivity medium, producing notch band response at its designed frequency. This notch band is shifted by varying the arm length of the CSRR using PIN diodes. This will result in tuning the bandwidth (BW) of the NB response of antenna, spanning from 1 GHz to 4.4 GHz, by retaining the central frequency at 6 GHz. The fractional bandwidth can be varied in a range of 16% to 73.3%, exhibiting an increase by a factor of 4.58. The antenna also exhibits switchable circular polarization (LHCP/RHCP) at 6 GHz for both UWB and narrowband responses. A compact tunable multiband Artificial Magnetic Conductor (AMC) unit cell is also designed and is used to construct a Phase Gradient Metasurface (PGM). The radiating beam of the antenna is steered using the PGM as a reflector to obtain a beam steering angle of $+36^\circ$ for LHCP and -44° for RHCP radiations. The antenna is a promising solution for applications which demand bandwidth switching & beam steering, such as cognitive radio services.

1. INTRODUCTION

The emerging requirements and rapid expansion, amidst the arena of all the wireless telecommunication technologies, urge for the design of compact antennas, having the capacity to handle multiple standards and multiple functionalities simultaneously. For applications such as Cognitive Radio (CR) service, where an abrupt change in data rate is expected to occur, the device should be able to tune its own bandwidth in order to attain efficient signal reception [1]. Such applications also require the antenna to switch its polarization sense and radiation pattern, so as to increase its efficiency and coverage. The suitable insertion of metamaterial configurations into the antenna can be cleverly used to alter its resonant characteristics, polarization, and radiation pattern, according to the application, at low cost and complexity.

In the preceding years, numerous designs of bandwidth reconfigurable, polarization reconfigurable, and beam steering antennas have been proposed according to requirements of wireless communication technology. In [1], the bandwidth of a patch antenna is tuned by electronically switching the slot-loaded PIN diodes, placed on the ground plane, but here, only the higher band edge is tuned. In [2], the lower and higher band limits of a Yagi-Uda antenna are independently tuned electronically, using resonator and slot-line techniques, respectively. In [3], beam tilting is achieved using a reconfigurable gradient phase metasurface, but in this design, the antenna structure has a large size. A PIN diode loaded circular loop patch antenna is proposed in [5], which is capable of tuning its resonant frequency and bandwidth, but this antenna is not suitable for UWB operation. A circularly polarized (CP), dual-band antenna is proposed in [9], which can independently control the polarization sense of its both resonant bands, by means of two interconnected split ring resonators. In [11], a beam-steerable slot antenna is presented, in which the radiating beam is tilted by switching a PIN diode, loaded across the parasitic slot near the radiating slot. The antenna proposed in [13] can switch between UWB and NB responses, but unable to tune the bandwidth of its narrow-band response. In [15], a coplanar waveguide (CPW) fed tri-band slot antenna is loaded with Split Ring Resonators (SRRs) having multiple micro-splits, for achieving CP. The antenna presented in [16] is capable of tuning its bandwidth, but unable to either switch its polarization sense or steer its radiation beam. The above-mentioned beam-steerable antennas are not capable of tuning its impedance bandwidth, while none of the bandwidth tunable antennas are capable of steering their beam. Also, the above-mentioned circularly polarized antennas are neither capable of tuning its impedance bandwidth nor steering its beam.

This work presents a compact, reconfigurable monopole circular patch antenna, which can electronically switch between UWB and NB responses, with a switchable sense of Right Hand Circular Polarization (RHCP) & Left Hand Circular Polarization (LHCP) radiation. The antenna is also capable of tuning the impedance bandwidth of NB response. A novel, compact, tunable multiband Artificial Magnetic Conductor (AMC) unit

* Corresponding author: Naveen Jacob (naveenjacob@yahoo.com).

cell is also designed and is used to form a phase gradient metasurface (PGM). The proposed antenna can steer its radiating beam using the PGM as a reflector.

The novelty of our work is that the proposed antenna can tune all the major antenna parameters independently, as per the application requirement. Hence, the antenna can singlehandedly manage multiple functionalities simultaneously, with better performance than other recent works.

In Section 2, the structure of the proposed bandwidth reconfigurable antenna is discussed, followed by its results. In Section 3, the design of a multiband tunable AMC unit cell is proposed. The design of PGM using this unit cell is also discussed in this section. The reconfigurable antenna is integrated with PGM, and the radiation characteristics are analyzed to exhibit the beam steering ability of the antenna, followed by the simulated and measured results. The antenna is fabricated and then tested.

2. DESIGN OF PROPOSED BANDWIDTH AND POLARIZATION RECONFIGURABLE ANTENNA

2.1. Theory and Technique Applied

Metamaterial properties can be accomplished by the inclusion of metallo-dielectric structures, such as Complementary Split Ring Resonator (CSRR)/Split ring Resonator (SRR), resulting in negative permittivity/negative permeability to attain a notch band on the desired frequency [9, 16]. Axial electric field excites the CSRR, which will induce oscillating currents between the two rings, to produce a resonance and forbid the propagation of the signal at the desired frequency.

Circular SRR/CSRR and their equivalent circuits are given in Chinmoy [17] by Saha and Siddiqui and [18] by Baena et al., and shown in Fig. 1, where "c" is the ring width; "d" is the inter-ring spacing; "r_o" and "r_i" are outer and inner ring radii, respectively.

The resonant frequency of SRR (f_{SRR}) is given by the following equation:

$$f_{SRR} = 1/2\pi\sqrt{LsCs} \tag{1}$$

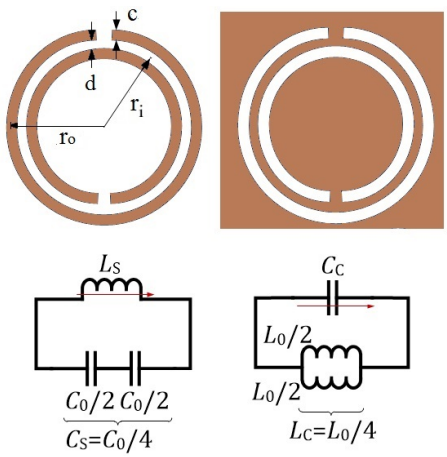

FIGURE 1. Circularly structured SRR and CSRR with their equivalent circuits (Dimensions are in mm).

where Cs and Ls are the effective capacitance and inductance in the equivalent circuit of SRR.

$$Ls = 0.0002l\left(2.303\log 10\left[\frac{4l}{c}\right] - 2.451\right)\ \mu\text{H} \tag{2}$$

where "l" is the length of the outer ring, and "c" is the width of the ring.

$$Cs = \left[\frac{\pi r_{avg}C_{pul}}{2} + \frac{\varepsilon 0ch}{2g}\right] \tag{3}$$

where "r_{avg}" is the average ring radius, "C_{pul}" the capacitance per unit length between the inner and outer rings of SRR, "h" the thickness of substrate, and "g" the split gap dimension of the ring.

The parameters of the CSRRs and SRRs in the circuit models are related due to duality, by the following equations:

$$Cc = 4\left(\frac{\varepsilon 0}{\mu 0}\right)Ls \tag{4}$$

$$C0 = 4\left(\frac{\varepsilon 0}{\mu 0}\right)L0 \tag{5}$$

From the above equations and the equations shown in Fig. 1, the values of effective Cc and Lc of CSRR can be calculated. The resonant frequency of CSRR (f_{CSRR}) can be obtained by the following equation:

$$f_{CSRR} = 1/2\pi\sqrt{LcCc} \tag{6}$$

where Cc and Lc are effective values of capacitance and inductance.

A CSRR of circular shape is designed and embedded on the antenna ground plane, as shown in Fig. 3, directly underneath the feed line, in order to maximize the coupling and produce a notch-band response at the desired frequency. If the length of the outer ring, "l", in Equation (2) can be electronically varied, then it will change the value of "Ls". This will change the effective capacitance "Cc" in Equation (4), thereby changing the frequency of resonance of CSRR, given in Equation (6). This will shift the notch band to a lower/higher frequency band, resulting in the tuning of the impedance bandwidth of narrow-band response of the antenna.

2.2. Antenna Structure and Design

A monopole antenna with a circular patch, having a partial ground plane, is the geometry considered for the proposed antenna. Fig. 2 shows the top surface, and Fig. 3 shows the bottom surface of the antenna. All measurements displayed are in mm. Material of the substrate selected is FR4, having $\varepsilon_r = 4.4$ and thickness 1.6 mm. The length and width of the substrate $L = W = 40$ mm. All the slots on the antenna are 0.2 mm wide. The 35 µm thick circular copper patch has a radius of 9 mm.

A CSRR is placed on the ground surface, below the feed line. The radius of the outer ring, $r_o = 2.6$ mm, radius of inner ring, $r_i = 2.2$ mm, and split gap dimension, $g = 0.2$ mm. Each ring

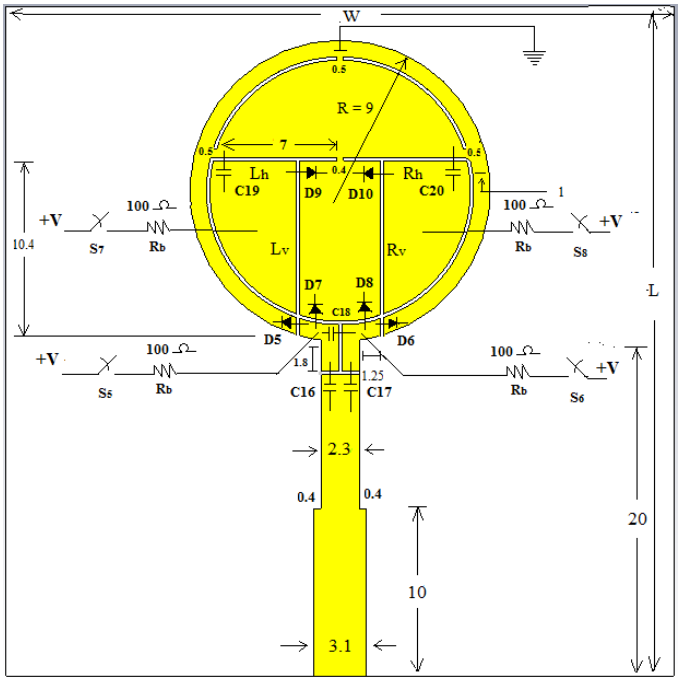

FIGURE 2. Top view — Antenna radiating patch with PIN diodes and biasing circuit (Dimensions are in mm).

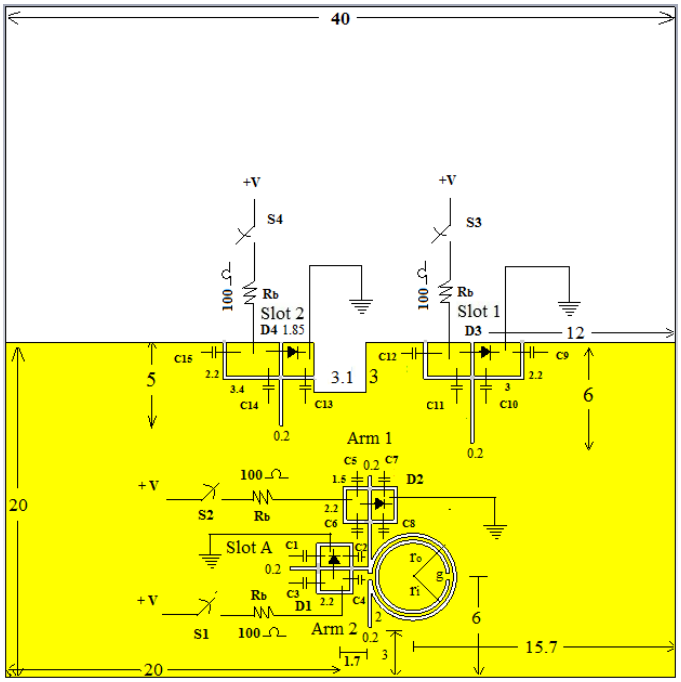

FIGURE 3. Bottom view — Antenna ground plane with PIN diodes and biasing circuit (Dimensions are in mm).

has a width of 0.2 mm. The rings are separated by a distance of 0.2 mm. Bandwidth is tuned using 4 PIN diodes, D1, D2, D3, and D4, as given in Fig. 3. Two slots named, Arm1 and Arm2, are connected to the CSRR. Arm1 can be electronically tuned using PIN diode D2 to vary the effective length "l" of the outer ring, thereby varying Ls. This will vary the effective capacitance, Cc, resulting in tuning the resonant frequency of CSRR as per Equation (6). Another slot, named Slot A, is also attached to the CSRR and loaded with PIN diode D1 and connected to switch S1. The length of Slot A extends across the feed line from beneath to achieve maximum coupling between the feed line and CSRR.

Switching ON the diode D1 will reduce the coupling between the feed line and CSRR, resulting in a UWB response. Switching OFF D1 increases the coupling and will result in an NB response at 6 GHz. Hence, D1 must be OFF for the remaining switching cases of NB responses. When D1 is switched OFF, the CSRR resonates and exhibits a stopband at 4 GHz. The slot "Arm1" is attached to the CSRR, loaded with diode D2, and connected to switch S1. When diode D2 is OFF, it will increase effective capacitance, Cc, which will shift the stopband, towards the lower band of frequency, 3.5 GHz, thereby changing the impedance bandwidth of the antenna.

Two additional slots, "Slot 1" & "Slot 2" are etched on the ground surface. Diode D3 is placed on "Slot 1" and diode D4 placed on "Slot 2", to tune the lower band and higher band edges of the NB bandwidth. D2 and D3 are connected to the battery through switches S3 and S4. Necessary slots are provided around the diodes to block DC while biasing. Surface Mount Device (SMD) capacitors, C1 to C15, are loaded across these slots to allow radio frequency (RF) to pass through the patch.

2.3. Tunable Circular Polarization

The mismatch in the polarization can result in signal loss and thereby reduce the performance of the antenna. One solution to improve the performance is to design a CP antenna. For this, the circular patch of the antenna is loaded with two vertical slots, L_v & R_v, and two horizontal slots, L_h & R_h, inside a circular slot having four gaps, each of 0.5 mm width as shown in Fig. 4. The circular slot is placed 1 mm. from the edge of the circular patch.

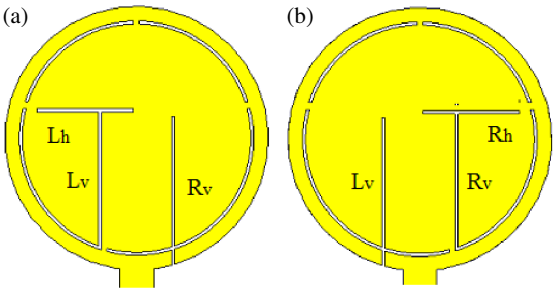

FIGURE 4. (a) LHCP configuration. (b) RHCP configuration.

Vertical slots are connected to the edge of the disc through the circular slot to obtain a switchable circular polarization, LHCP/RHCP, at 6 GHz. Two orthogonal modes are excited in phase quadrature due to the presence of the T-shaped slots, to attain CP. All slot lengths are fine-tuned to optimize the CP, centered at 6 GHz. Slot positions for LHCP and RHCP conditions are shown, respectively, in Fig. 4.

Six diodes, D5 to D10, connected to battery through switches S5 to S8, are positioned across the slots for switching both the polarization senses of the radiation, as shown in Fig. 2. Switching ON diodes D5, D7, D10 and switching OFF diodes D6, D8,

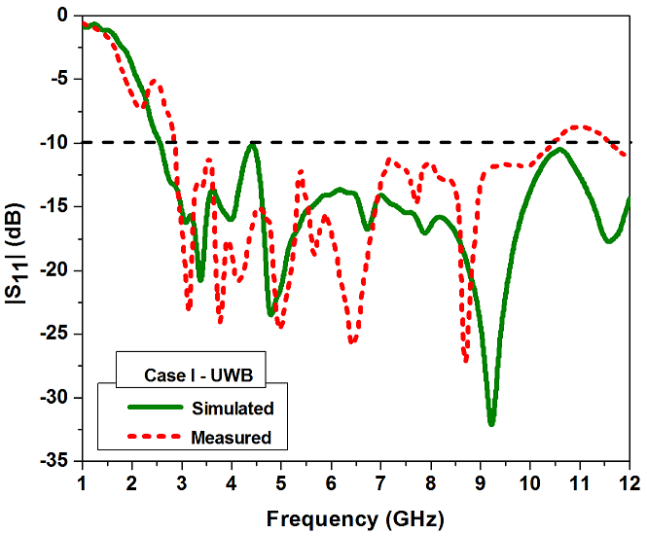

FIGURE 5. Simulated and measured $|S_{11}|$ for Case-I — UWB response.

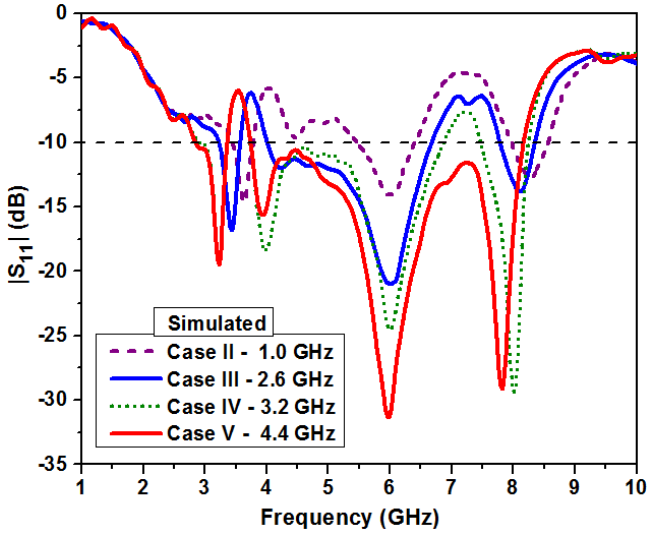

FIGURE 6. Simulated result of $|S_{11}|$ — NB responses of Case — II, III, IV, and V.

TABLE 1. Diode switching configurations for tuning polarization and bandwidth of the tunable antenna.

Cases	Diode switching configurations										Sense of	Axial Ratio	Bandwidth
	D1	D2	D3	D4	D5	D6	D7	D8	D9	D10	Polarization at 6 GHz	BW (GHz) & (%)	(GHz) & (%)
Case I	1	1	1	1	1	0	1	0	0	1	LHCP	0.9 (15 %)	UWB (2.6–12)
					0	1	0	1	1	0	RHCP	1.36 (22.7 %)	
Case II	0	1	0	1	1	0	1	0	0	1	LHCP	1 (16.7 %)	1 (16 %)
					0	1	0	1	1	0	RHCP	1 (16.7 %)	
Case III	0	1	1	1	1	0	1	0	0	1	LHCP	1 (16.7 %)	2.6 (48.8 %)
					0	1	0	1	1	0	RHCP	1 (16.7 %)	
Case IV	0	0	1	1	1	0	1	0	0	1	LHCP	1 (16.7 %)	3.2 (61 %)
					0	1	0	1	1	0	RHCP	1 (16.7 %)	
Case V	0	0	1	0	1	0	1	0	0	1	LHCP	1 (16.7 %)	4.4 (73.3 %)
					0	1	0	1	1	0	RHCP	1 (16.7 %)	

D9 will connect the slot R_v to the boundary of the patch, and form the configuration shown in Fig. 4(a), resulting in LHCP radiation. Similarly, switching ON diodes D6, D8, D9 and switching OFF diodes D5, D7, D10 will connect the slot L_v to the boundary of the patch and form the configuration shown in Fig. 4(b), resulting in RHCP radiation. SMD capacitors C16 to C20 are placed across the slots to allow RF to pass through the patch, while blocking DC.

2.4. Biasing the Antenna and Simulation Analysis

Computer Simulation Technology (CST) Microwave Studio is used for the simulation analysis. The PIN diode used in this research work is MADP-000907-14020W. Parametric values of PIN diode used for the simulation study are extracted from its equivalent circuit.

The biasing circuit used for diodes is shown in Fig. 2 and Fig. 3. For blocking DC bias current, 20 SMD capacitors (GQM1885C1H101GB01D), C1 to C20, each having capacitance of 100 pF, are used. Resistance (R_b) of 100 Ω is used for limiting the diode current. Switches S1 to S8 are used to connect DC power supply. Diodes on the antenna plane and ground plane are separately powered by two 3 V DC supplies.

2.5. Simulated and Measured Results

The results of antenna simulation and fabrication, depending upon the various cases of diode switching conditions are presented in Table 1. "ON" state of the diode is represented by "1" and "OFF" state by "0". For each case of switching configurations of diodes D1 to D4, there are two sub-configurations for diodes D5 to D10, which decides the circular polarization sense (RHCP/LHCP).

In diode switching case I, since D1 is in "ON" state, the coupling of the CSRR with the feed line decreases, which results in UWB response (2.6 GHz to 12 GHz), as shown in Fig. 5. Axial Ratio (AR) BW of 900 MHz, (15% fractional AR band width) for LHCP and 1.36 GHz (22.7% fractional AR BW) for RHCP are obtained.

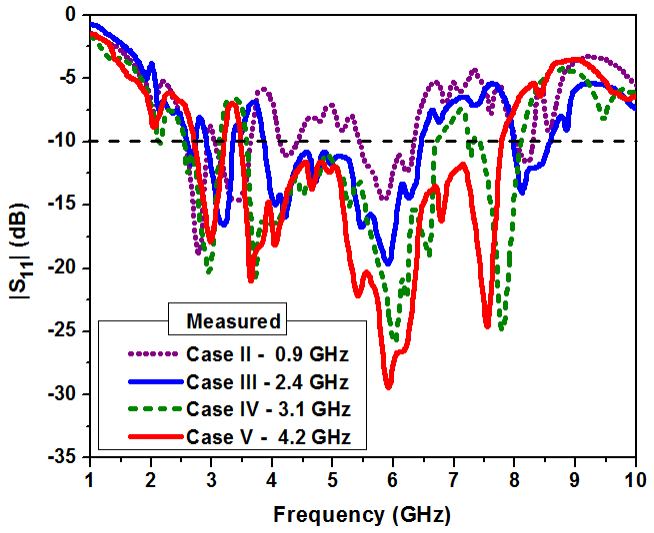

FIGURE 7. Measured result of $|S_{11}|$ — NB responses of Case — II, III, IV, and V.

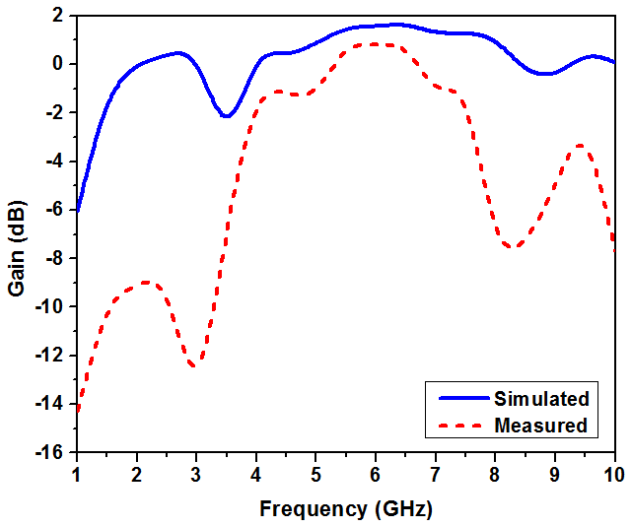

FIGURE 8. Gain of the CP monopole antenna.

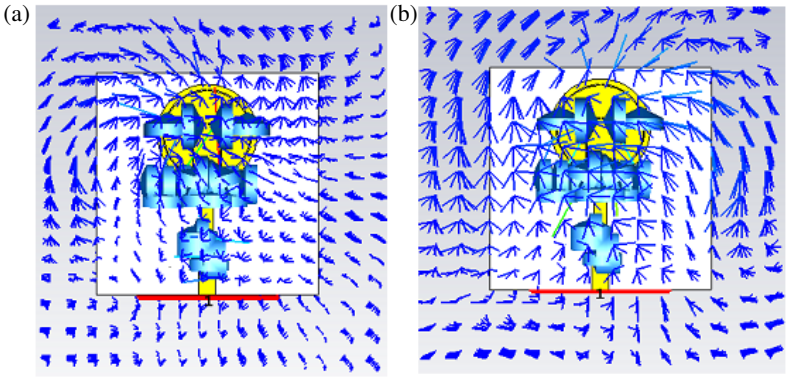

FIGURE 9. E-field distributions. (a) LHCP. (b) RHCP.

In diode switching case II, D1 is switched OFF. Hence, the "Slot A", underneath the feed line, modifies the distribution of current, which results in NB, with band-center at 6 GHz. The CSRR resonates and produces a stopband at 4 GHz. In this case, D3 is also switched OFF. Hence, the "Slot 1" generates another stopband at 5 GHz, which limits the bandwidth of NB to 1 GHz, as given in Fig. 6 & Fig. 7. A fractional bandwidth of 16% is attained. In diode switching case III, when D3 is switched ON, the stopband at 5 GHz vanishes, resulting in lowering the stopband at 4 GHz to 3.8 GHz. Thus, the bandwidth of NB is enhanced to 2.6 GHz, as given in Fig. 6 & Fig. 7. A fractional bandwidth of 48.8% is obtained. In diode switching case IV, D2 is switched OFF, and hence, the slot length of "Arm1", attached to CSRR, increases, thereby increasing the capacitance, *Cc*, given in Equation (6). Hence, the notch band again moves to lower frequency of 3.5 GHz, whereby, the bandwidth again increases to 3.2 GHz, as given in Fig. 6 & Fig. 7. A fractional impedance bandwidth of 61% is attained. In diode switching case V, since D4 is switched OFF, "Slot 2" alters the distribution of current, resulting in moving the higher band edge of the NB response from 6.9 GHz to 8.1 GHz, whereby, the bandwidth increases further, to 4.4 GHz, as given in Fig. 6 & Fig. 7. A fractional bandwidth of 73.3% is attained.

Figure 8 shows that the simulated gain of the reconfigurable CP monopole antenna is 1.5 dB, and measured gain is 1 dB. The reason for the low value of gain is that the antenna is in low profile and uses a FR4 substrate. Also, the antenna uses a half ground plane, which leads to back scattering and adversely affects the radiation pattern and gain. In addition to this, the presence of resistive, capacitive, and inductive components inside the equivalent circuit of PIN diode and biasing network also adversely affects the gain.

Figures 9(a) and (b) show the distribution of the electric field for LHCP & RHCP, respectively at 6 GHz. Fig. 10 and Fig. 11 display the axial ratios of the antenna for RHCP and LHCP, respectively at 6 GHz, with 16.7% fractional axial ratio bandwidth, for all narrow-band switching conditions.

The simulation result shows that both the lower and higher band edges are tuned using electronic switching through which the fractional impedance bandwidth can be varied from 16% to 73.3%. Thus, the impedance bandwidth is increased by a factor of 4.58.

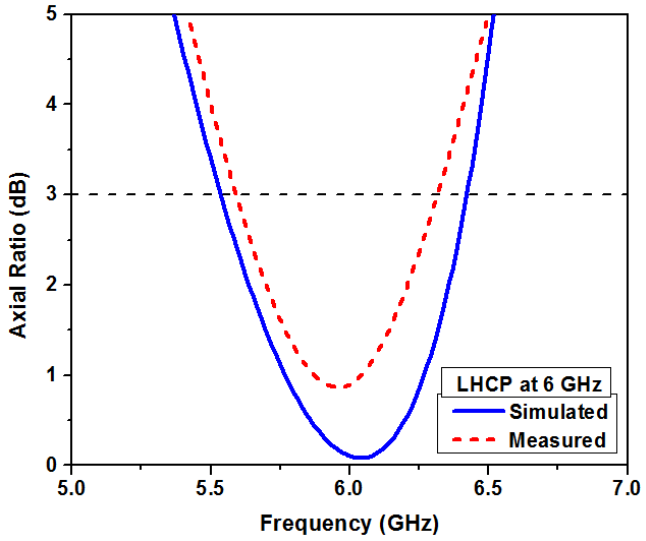

FIGURE 10. Axial ratio — LHCP.

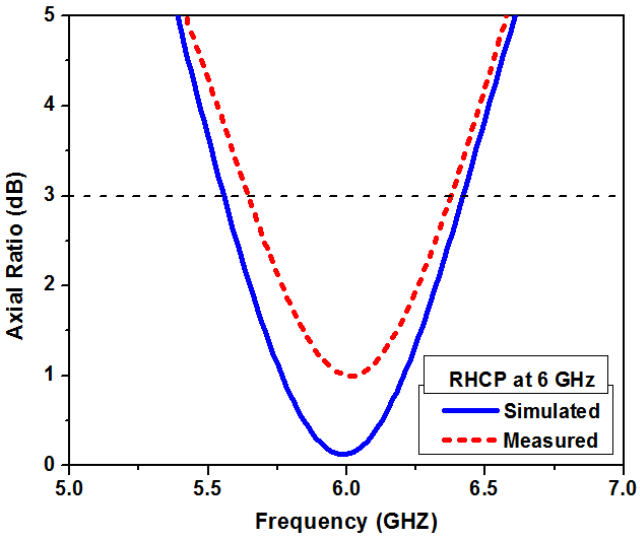

FIGURE 11. Axial ratio — RHCP.

3. DESIGN OF TUNABLE MULTIBAND AMC UNIT CELL METASURFACE FOR BEAM STEERING

This section details the design of a miniaturized, multiband reconfigurable AMC unit cell. This is followed by the discussion on the design of a zero phase metasurface (ZPM) and also a phase gradient metasurface (PGM), with the designed unit cell, which can be smartly utilized for enhancing the gain and steering the beam of the CP monopole antenna.

3.1. Proposed AMC Unit Cell --- Theory and Design

The conventional square-shaped loop AMC unit cell exhibits dual-band reflection phase-frequency response in the desired frequency band. In this work, we have modified the conventional square loop unit cell to obtain a multiband, tunable frequency response, with a reduced ground plane size of $W_s = L_s = 11$ mm on an FR4 substrate of thickness 3.2 mm, as given in Fig. 12. The conventional square loop unit cell is equivalent to a parallel resonant LC circuit as given in [19] by Afridi et al. Its geometry and dimensions decide the frequency of resonance, f_r, given in Equation (7).

$$fr = 1/2\pi\sqrt{L_e C_e} \tag{7}$$

where C_e and L_e are surface capacitance and inductance, given by Equations (8) and (9).

$$L_e = \mu o \mu r t \tag{8}$$

$$C_e = \frac{W_p(\varepsilon r + 1)\varepsilon o}{\pi} \cosh^{-1}\left(\frac{b+g}{g}\right) \tag{9}$$

where "t" is the substrate thickness, "W_p" the outside patch width, and "g" the space between the patches of the neighboring unit cell. The factor "$(b+g)$" is called "array period", in which "b" can have different values. Zero phase reflection for lower resonance and higher resonance bands are influenced when $b = W_p$ and $b = W_i$, respectively, where "W_i" is the width of the patch inside the square loop.

For shifting the resonant frequency to the lower band, the value of L_e or C_e, in Equation (7), has to be increased. To increase the L_e, substrate thickness should be increased. This will lead to an increase in the size of the unit cell, which is not desirable.

To increase the value of C_e, without increasing unit cell size, the effective values of W_p & W_i need to be altered. The technique involves routing the square loop in a meandered pattern over the copper patch to increase its electrical length while maintaining a compact physical size. This will increase the electrical length of inner patch, resulting in the increase of effective W_i, without varying the overall unit cell size. Moreover, two long horizontal slots, T_{hr} & B_{hr}, are loaded on the top and bottom spaces of the outer patch, which will in-

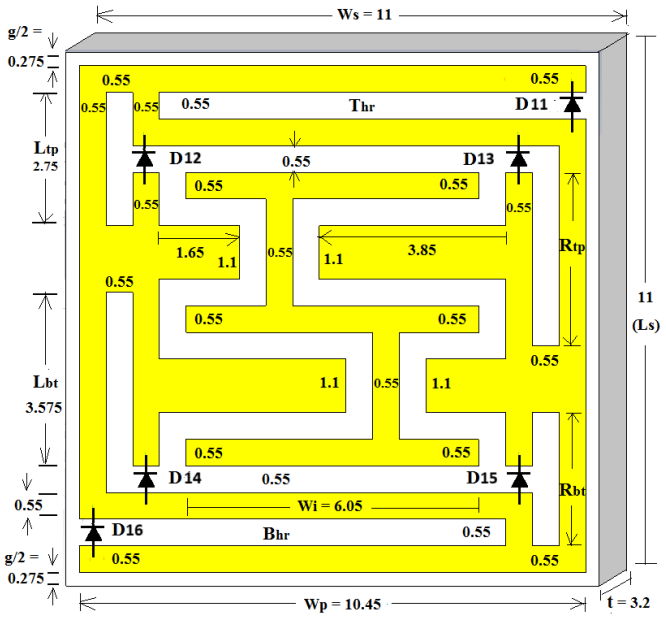

FIGURE 12. Proposed reconfigurable unit cell (Dimensions are in mm).

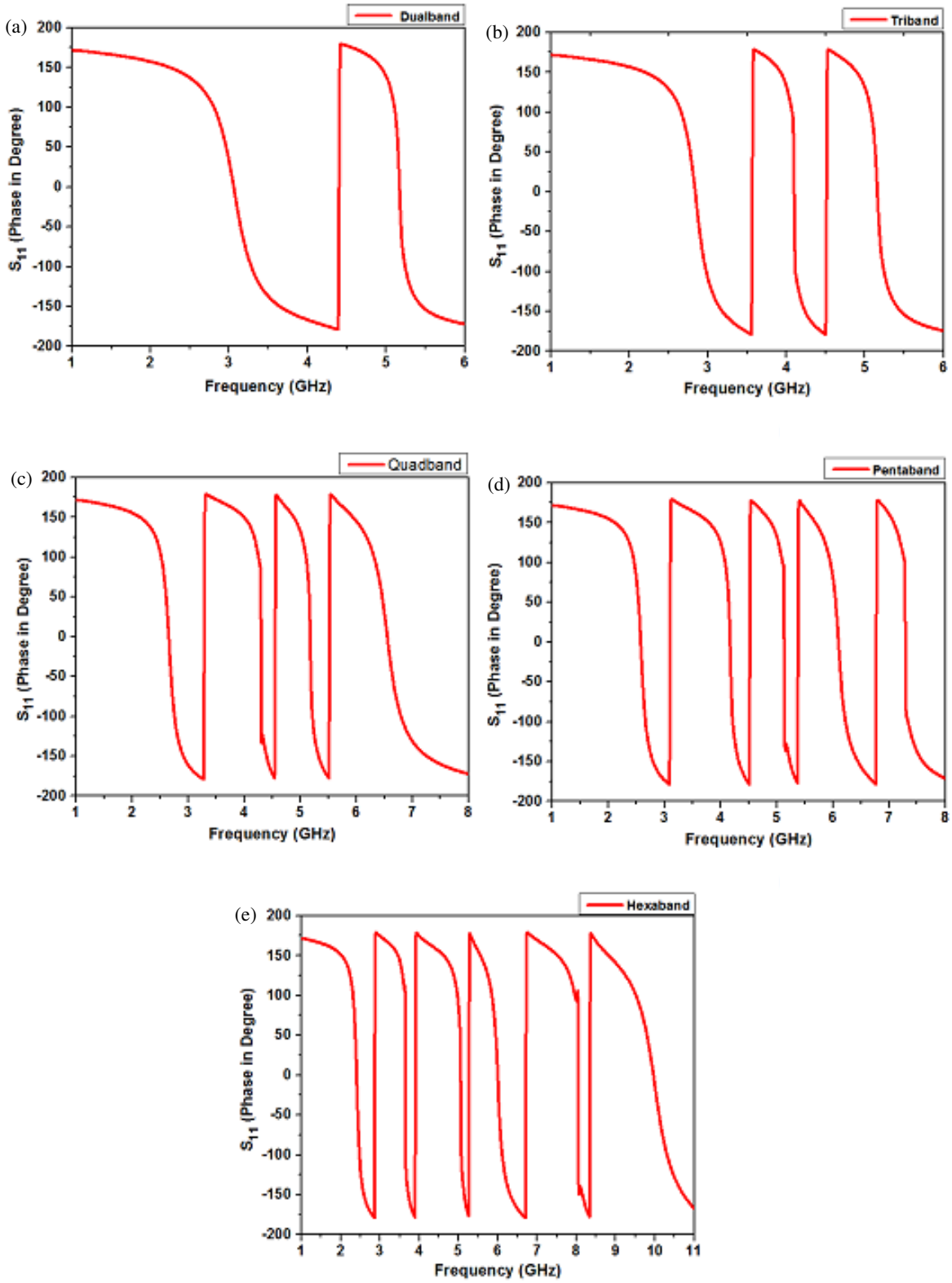

FIGURE 13. Reflection phase for (a) Case 1 — Dual band, (b) Case 2 — Tri band, (c) Case 3 — Tetra band, (d) Case 4 — Penta band, (e) Case 5 — Hexa band.

crease the electrical length of outer patch, resulting in the increase of effective W_p. This will result in the occurrence of a greater number of resonance bands towards a lower frequency band around the narrowband operating frequency (6 GHz) of the antenna. Besides this, four slots, $R_{bt} = L_{tp} = 2.75$ mm, $R_{tp} = L_{bt} = 3.575$ mm, are loaded at the four corners of the meandered loop and connected using PIN diodes, as given in Fig. 12. D11 to D16 are the 6 PIN diodes deployed for vary-

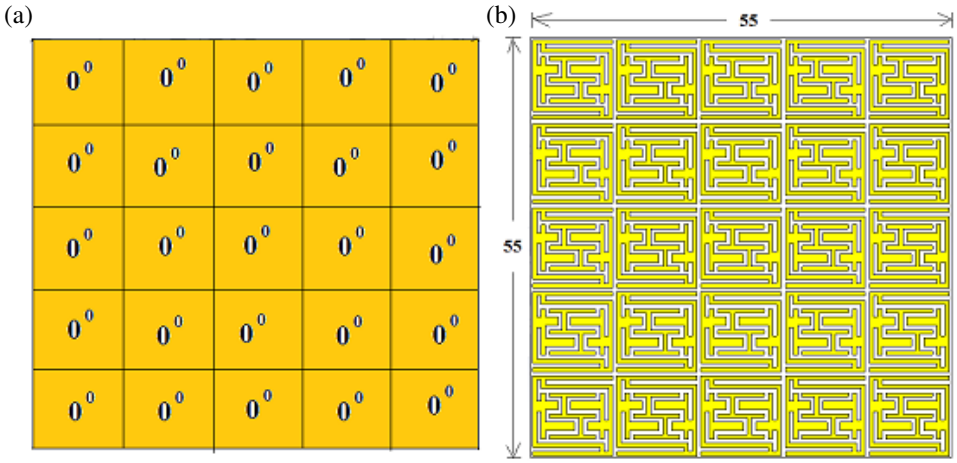

FIGURE 14. ZPM at 6 GHz. (a) Diagrammatic representation. (b) Metasurface.

TABLE 2. Diode switching configurations for tuning the reflection phase of unit cell AMC.

Cases	Diode switching configurations						No. of Bands	Frequency at 0°	Band Width
	D11	D12	D13	D14	D15	D16	(GHz)	Reflection Phase (GHz)	(MHz)
Case 1	1	1	1	1	1	1	Dual-band	3, 5.2	412, 127
Case 2	1	1	0	0	1	1	Tri-band	2.8, 4.1, 5.2	250, 50, 150
Case 3	0	1	1	1	1	0	Tetra-band	2.6, 4.3, 5.2, 6.5	210, 40, 100, 380
Case 4	0	1	1	0	1	0	Penta-band	2.6, 4.2, 5.2, 6, 7.2	170, 100, 35, 230, 40
Case 5	0	0	0	0	0	0	Hexa-band	2.4, 3.6, 5.1, 6.0, 8.1, 9.9	140, 30, 80, 210, 30, 690

ing effective value of W_p/W_i and thereby tuning the reflection phase and number of bands.

3.2. Simulation Results of AMC Unit Cell

The simulated values of the reflection phase coefficients, given in Fig. 13, for five different diode switching conditions, are presented, as given in Table 2. The "ON" state of the diode is denoted using "1" & "OFF" state using "0".

3.3. Design of Zero Phase Reflecting Metasurface (ZPM)

The AMC unit cell in Fig. 12, with $R_{bt} = L_{tp} = 2.75$ mm, $R_{tp} = L_{bt} = 3.575$ mm, having all diodes in "OFF" condition or all diodes removed (diode switching case 5), is selected for the design of Zero Phase Metasurface (ZPM). It has six phase reflection bands in which one band has 0° phase reflection at the antenna operating frequency, 6 GHz, as shown in Fig. 13(e). Twenty five such unit cells, under this configuration, are used to design a 5×5 array ZPM of size 55 mm $\times$ 55 mm $\times$ 3.2 mm, as shown in Fig. 14.

3.4. Antenna Gain Enhancement Using ZPM

Analyzing the results of reconfigurable CP antenna gain given in Fig. 8, it is evident that the gain is very small. One of the reasons is that the back scattering of radiation occurs because of the presence of a partial ground plane of the antenna. In order to redirect the back radiation, the 5×5 array ZPM, designed in section 3.3, is placed under the ground plane of the antenna, at a distance $d = \lambda/2$, which is 25 mm, as shown in Fig. 15 and Fig. 16. Here, λ is the wavelength of antenna operating frequency, 6 GHz.

Every unit cell forming the metasurface provides in-phase reflection at 6 GHz, and hence, the reflected radiation undergoes phase addition resulting in enhanced gain. Fig. 17 shows that the simulated gain of the reconfigurable CP monopole antenna with ZPM is 6 dB, and measured gain is 4 dB. An improvement of 4.5 dB simulated gain is attained. Simulation results show that the antenna, backed by ZPM, radiates a single beam, in the direction $-12°$ to the normal, for RHCP and $+10°$ to the normal, for LHCP switching conditions as shown in Fig. 22 and Fig. 23. Corresponding measured values after fabrication are $-24°$ and $+18°$, respectively, as shown in Fig. 24 and Fig. 25. Radiation pattern corresponds to the case III diode switching condition, given in Table 1.

3.5. Parametric Study of Unit Cell AMC and Design of Phase Gradient Metasurface (PGM)

The AMC unit cell, having all diodes "OFF" condition or all diodes removed (diode switching case 5), is considered for the parametric test. The reflection phase occurring at 6 GHz alone

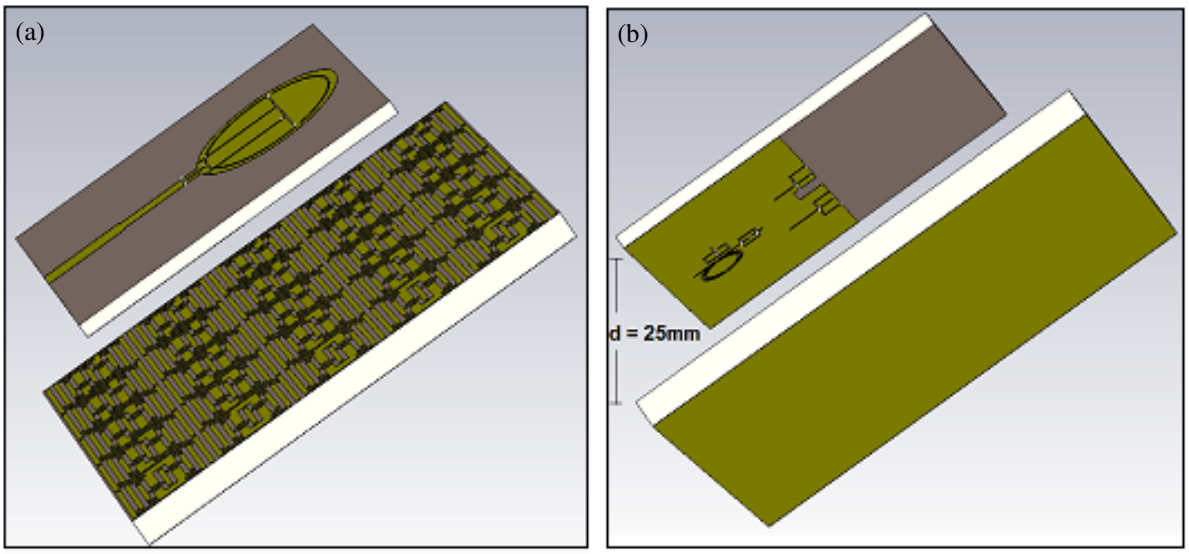

FIGURE 15. Antenna backed by ZPM. (a) Side view. (b) Back view.

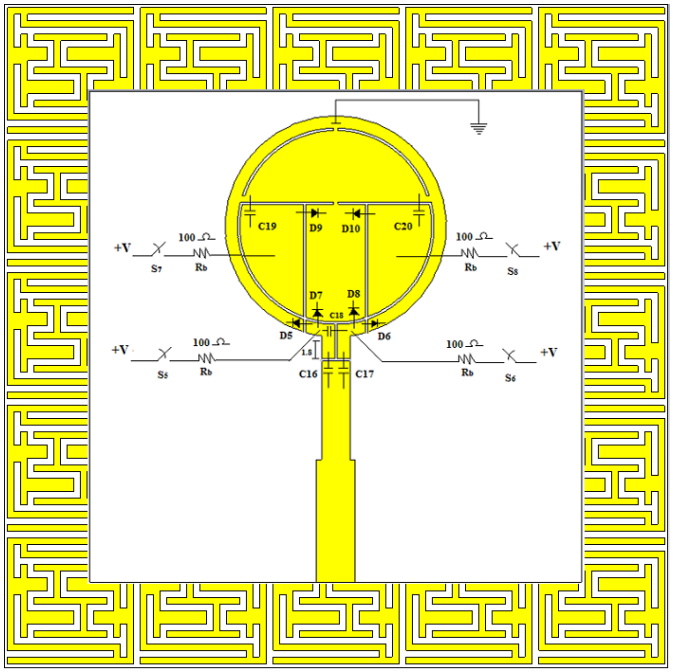

FIGURE 16. Antenna backed by ZPM — Front view.

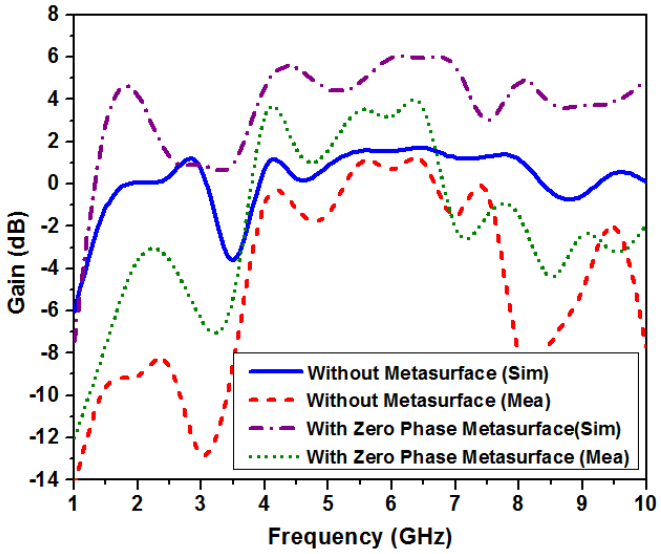

FIGURE 17. Antenna gain, with/without metasurface.

can be tuned independently, between $-180°$ and $+180°$, without varying the phase of reflection occurring at other frequencies. This can be achieved by varying effective capacitance C_e, of the meandered loop, given in Equation (9).

For realizing this, the slot lengths, $R_{bt} = L_{tp} = 2.75\,\text{mm}$, is kept constant, and the lengths of the slots, R_{tp} and L_{bt}, alone are varied equally, without changing any other dimensions.

The plot in Fig. 18 displays the variation of reflection phase at 6 GHz, according to the variation in slot lengths, R_{tp} and L_{bt}. It is shown that the phase variation is almost linear from $+180°$ to $-180°$.

Figure 19 shows that, for some selected values of lengths of the slots, L_{bt} & R_{tp}, the reflection phase at 6 GHz can be tuned through $-120°$, $-60°$, $0°$, $+60°$, and $+120°$, by maintaining the reflection phase at remaining frequencies, nearly constant.

Five unit cells, each having different values of lengths of slots, L_{bt} & R_{tp}, selected as $L_{bt} = R_{tp} = 4.5\,\text{mm}$, $L_{bt} = R_{tp} = 3.9\,\text{mm}$, $L_{bt} = R_{tp} = 3.6\,\text{mm}$, $L_{bt} = R_{tp} = 2.9\,\text{mm}$ and $L_{bt} = R_{tp} = 1.4\,\text{mm}$, are separately designed to obtain five different reflection phases, $-120°$, $-60°$, $0°$, $+60°$, and $+120°$ at 6 GHz. They are arranged in a 5×5 array, for the design of Phase Gradient Metasurface (PGM), as given in Fig. 20. This metasurface has an overall size $55\,\text{mm} \times 55\,\text{mm} \times 3.2\,\text{mm}$. The designed PGM is suitable to integrate with the proposed antennas for beam steering applications.

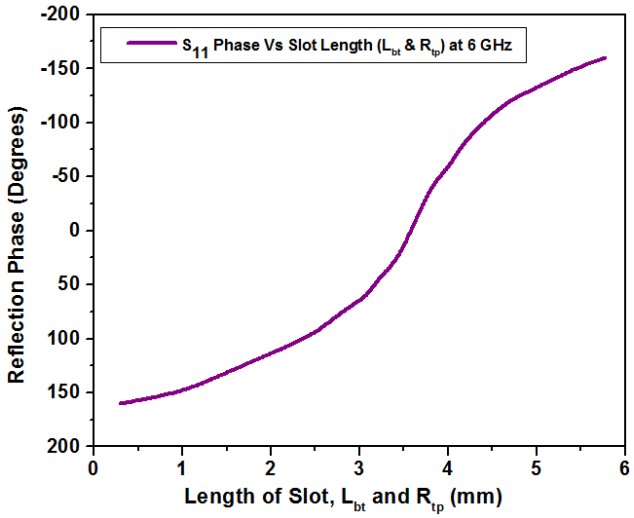

FIGURE 18. Reflection phase vs. slot length (R_{tp} and L_{bt}) at 6 GHz.

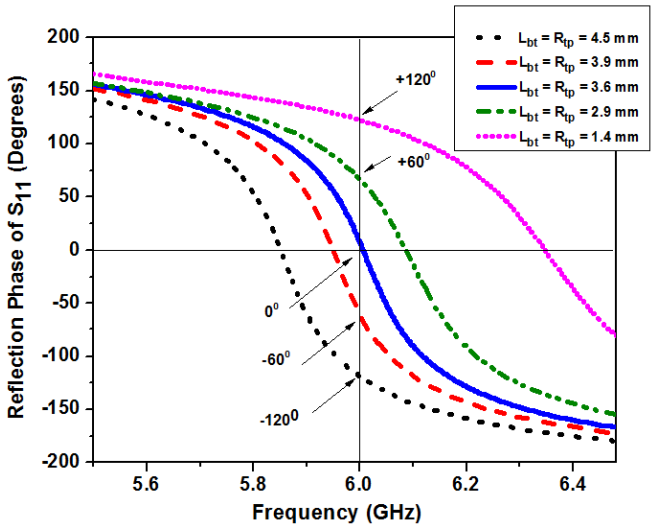

FIGURE 19. Variation in phase of reflection at 6 GHz, in diode switching Case-V, for different values of slot length, R_{tp} and L_{bt}.

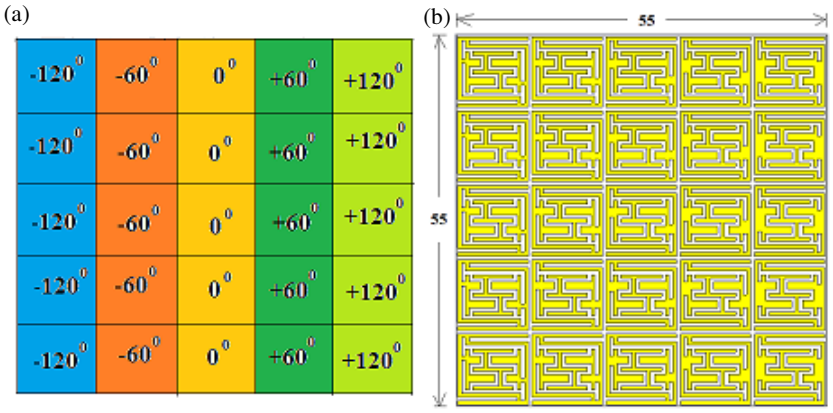

FIGURE 20. PGM at 6 GHz. (a) Diagrammatic representation. (b) Metasurface.

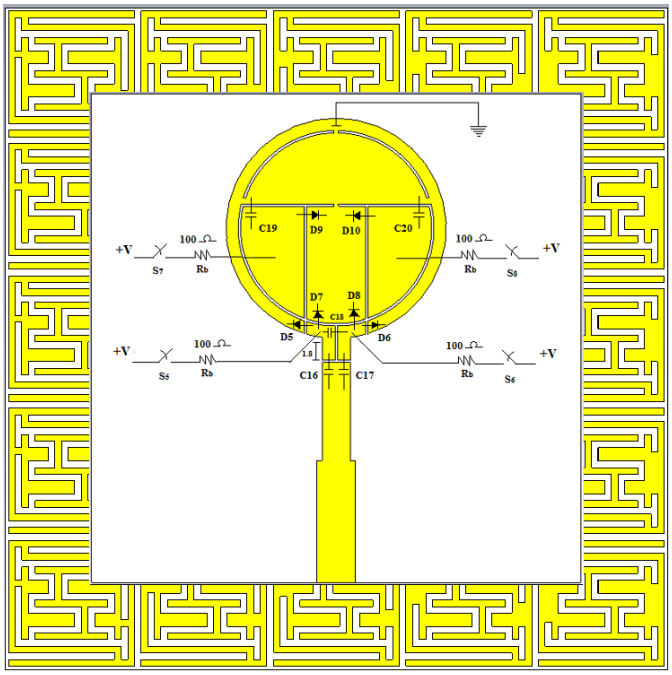

FIGURE 21. Antenna integrated with PGM — Front view.

3.6. Antenna Beam Switching Using PGM

A normally incident wave gets reflected by a linear gradient phase ($d\varphi/dx$) metasurface, at an angle θ_r, which relies on the magnitude of the phase gradient [3, 10]. The PGM designed in Section 3.5 is placed beneath the antenna ground plane, at a distance $d = 25$ mm, as given in Fig. 21. The PGM induces a progressive phase shift to the incident wave across its surface, which alters the direction of the wave front. This will reflect the wave to a desired angle, resulting in beam steering, as shown in Fig. 22 and Fig. 24, for both LHCP and RHCP polarization senses.

Simulated results show that, when the PGM is placed under the antenna, the radiating beam gets tilted to $-27°$ to the normal, under the diode switching condition for RHCP radiation and $+23°$ to the normal, under the diode switching condition for LHCP radiation, as given in Fig. 22 and Fig. 23. Hence, an overall beam steering range of 50° is achieved during simulation using both LHCP and RHCP switching conditions. The corresponding values measured after fabrication are $-44°$ to the normal for RHCP radiation and $+36°$ to the normal for LHCP radiation, as given in Fig. 24 and Fig. 25. Hence, an overall beam steering range of 80° is achieved after measure-

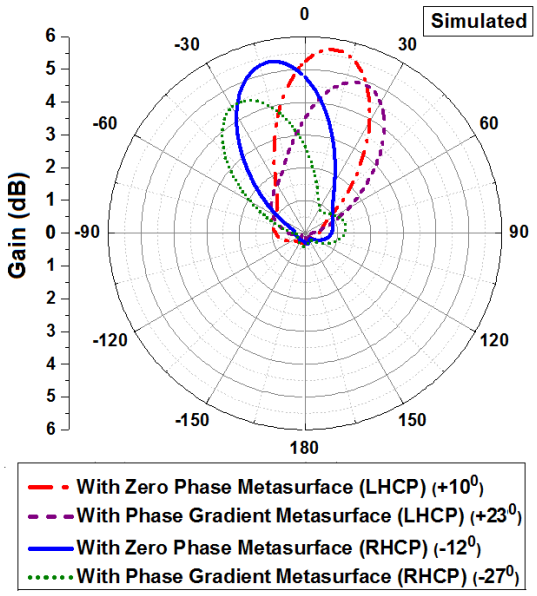

FIGURE 22. Simulated beam steering for RHCP and LHCP at 6 GHz (Polar plot).

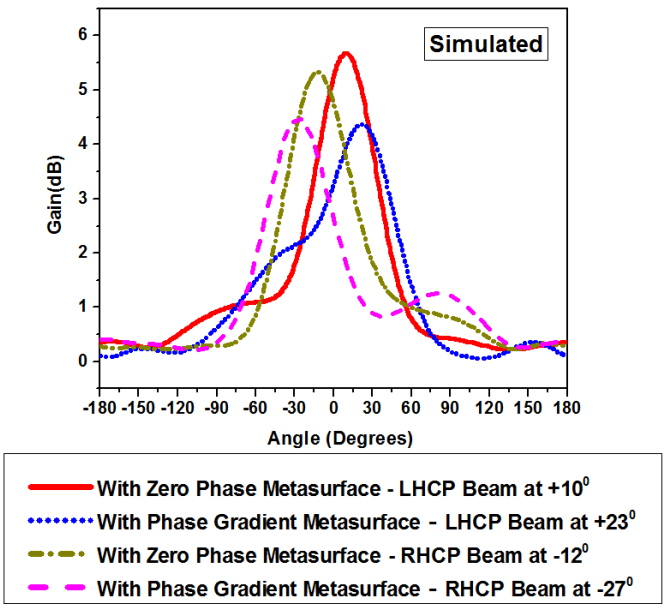

FIGURE 23. Simulated beam steering for RHCP and LHCP at 6 GHz (2D plot).

TABLE 3. Comparative analysis of the proposed work with related works on bandwidth tunable antenna.

Ref.	Parameters						Gain (dB)
	Antenna Dimensions (mm)	Type of tuning and No. of tuning elements	Bandwidth tuning ranges and fractional BW variation of NB	Tunable Polarization Sense	Beam switching ability & range	Factor by which % BW increased	
[1]	56 × 54	7 PIN diodes	(810–1870) MHz (43%–76%)	Nil	Nil	1.77	—
[2]	36 × 44	7 PIN diodes	(900–4700) MHz (18%–72%)	Nil	Nil	4	—
[7]	75 × 65	—	Nil	LHCP & RHCP	Nil	—	3.4
[8]	40 × 40	3 PIN diodes & 1 Capacitor	Nil	LP, LHCP & RHCP	Nil	—	7.5
[10]	34 × 28	Mechanical	Nil	Nil	−29° & +34°	—	7
[11]	70 × 70	2 PIN diodes	Nil	Nil	−36° to +36°	—	9.3
[12]	150 × 150	72 PIN diodes	Nil	Nil	−22° to +22°	—	10.4
[14]	120 × 120	Fluid (Water)	Nil	Nil	−20° to +20°	—	5.7
[20]	338 × 32	10 PIN diodes	Nil	Nil	−48° to +50°	—	12
[21]	MIMO Antenna 44 × 44, 75 × 75	8 PIN diodes	Nil	LP, LHCP & RHCP	Nil	—	5.7
[22]	28 × 28	72 PIN diodes	Nil	Nil	−57° to +57°	—	8.47
This work	**40 × 40**	**16 PIN diodes**	**(1–4.4) GHz (16%–73.3%)**	**LHCP & RHCP**	**-44° & 36°**	**4.58**	**6**

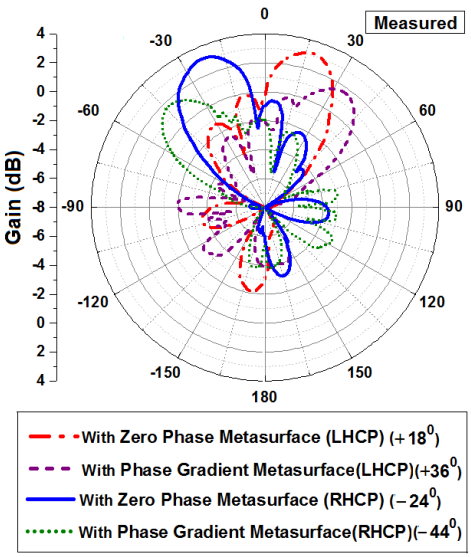

FIGURE 24. Measured beam steering for RHCP and LHCP at 6 GHz (Polar plot).

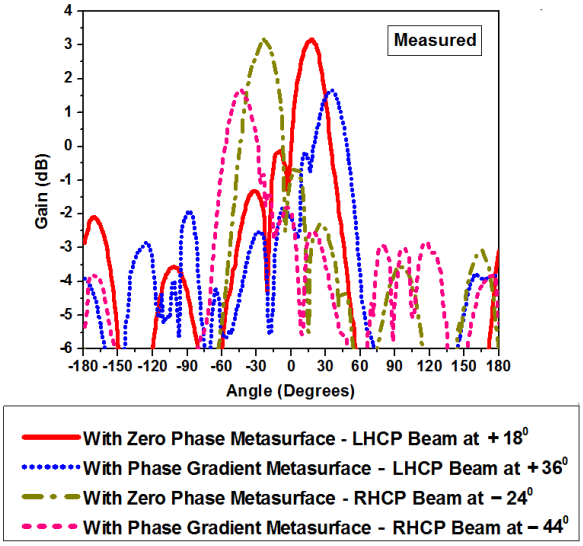

FIGURE 25. Measured beam steering for RHCP and LHCP at 6GHz (2D plot).

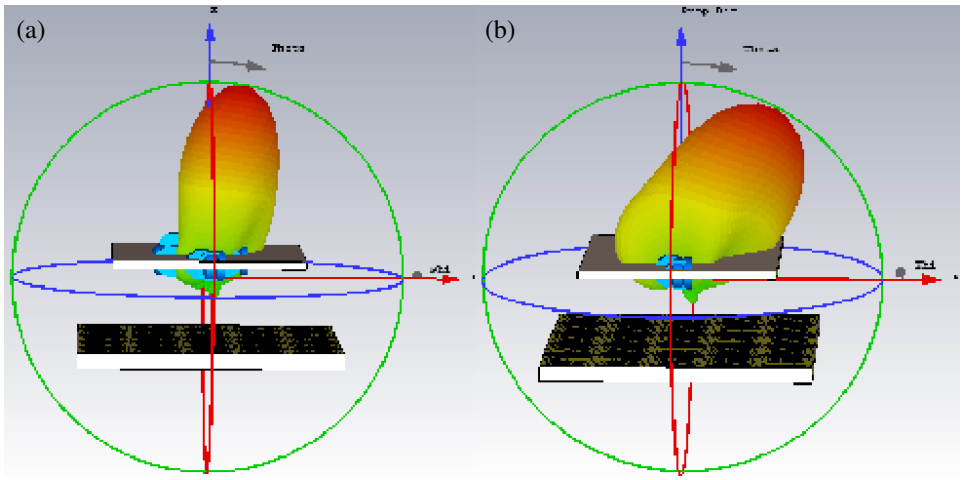

FIGURE 26. 3D view of simulated beam steering. (a) With ZPM (LHCP at $+10°$). (b) With PGM (LHCP at $+23°$).

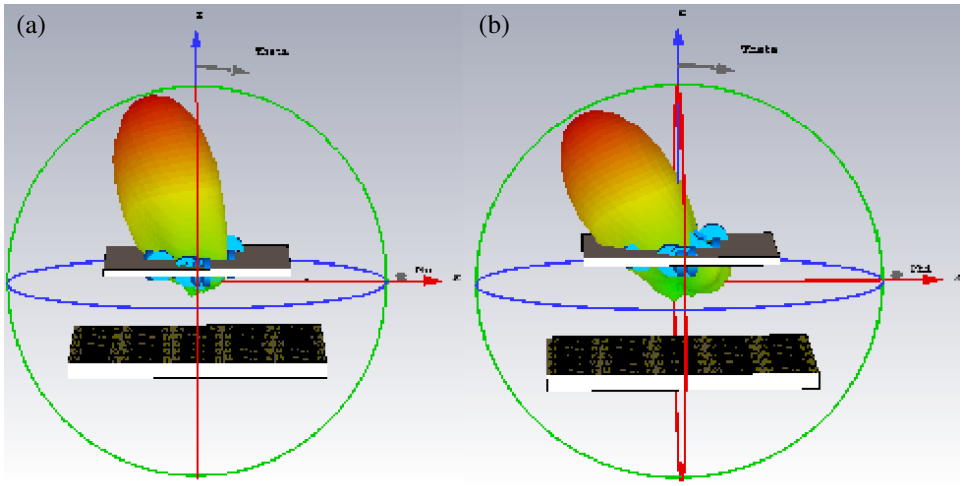

FIGURE 27. 3D view of simulated beam steering. (a) With ZPM (RHCP at $-12°$). (b) With PGM (RHCP at $-27°$).

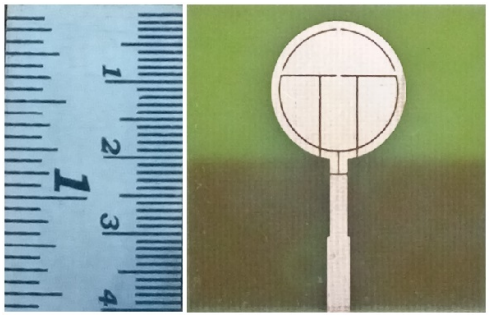

FIGURE 28. Fabricated antenna — Front view.

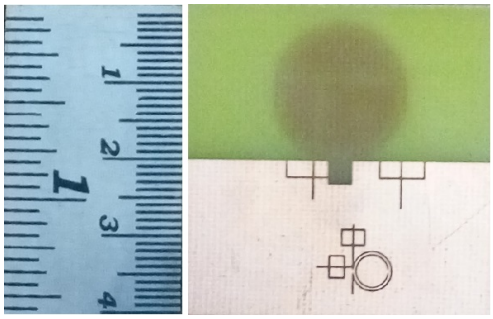

FIGURE 29. Fabricated antenna — Back view.

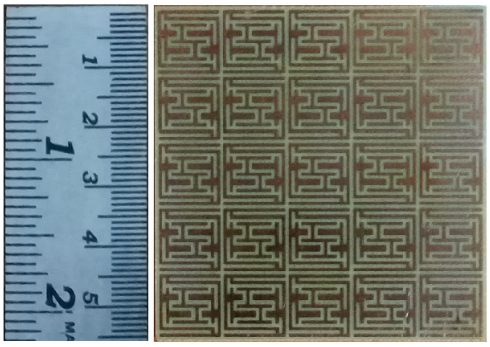

FIGURE 30. Fabricated ZPM — Front view.

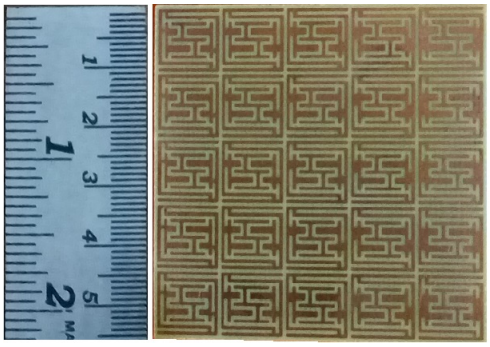

FIGURE 31. Fabricated PGM — Front view.

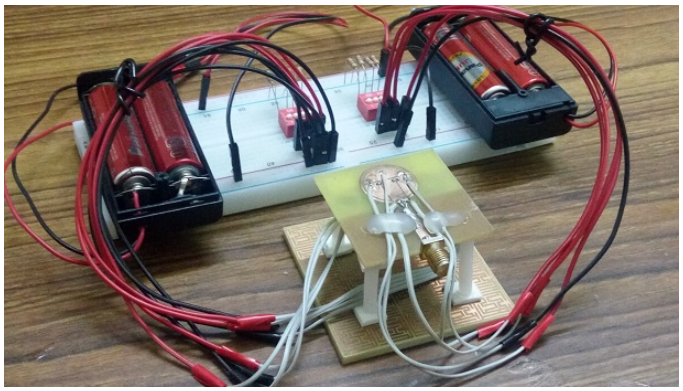

FIGURE 32. Fabricated antenna backed by metasurface, along with a biasing circuit.

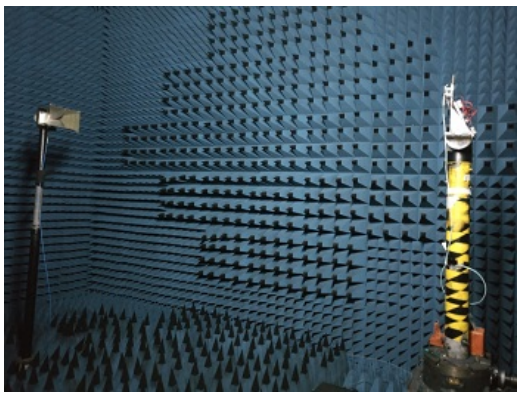

FIGURE 33. Antenna setup in anechoic chamber for parametric measurements.

ment using both LHCP and RHCP switching conditions. 3D views of the beam steering for both LHCP and RHCP are shown in Fig. 26 and Fig. 27.

The discrepancies between simulated and measured results, including the elevated side lobe level (SLL), occur due to the presence of electronic components and biasing network, which cause the variation in measured result. In addition to this, the tolerance related to fabrication and SMA connected probe feed may also lead to the variation in measured result.

This research work is compared with related preceding works and tabulated in Table 3, which reveals that the proposed reconfigurable antenna exhibits better performance than other similar works.

4. FABRICATED ANTENNA AND MEASUREMENT SETUP

Front and back views of the fabricated antenna are shown in Fig. 28 and Fig. 29.

The fabricated Zero Phase Metasurface (ZPM) and Phase Gradient Metasurface (PGM) are shown in Fig. 30 and Fig. 31.

The fabricated antenna and its biasing circuit, along with switching arrangements, on a breadboard are shown in Fig. 32. Diodes on the antenna plane and ground plane are separately powered by two 3 V DC supplies, connected through a series resistance of 100 Ω, for current limiting.

The fabricated antenna installed in an anechoic chamber for parametric measurements is shown in Fig. 33.

5. CONCLUSION

A bandwidth reconfigurable, circularly polarized antenna is proposed, which can be electronically switched from UWB to NB response at 6 GHz. The fractional impedance bandwidth of the NB can be tuned in the range of 16% to 73.3%, resulting in an increase of BW by a factor of 4.58. The antenna also exhibits both LHCP and RHCP polarization senses at 6 GHz based on different switching conditions. A multi-band, tunable AMC unit cell is designed, which is also capable of independent tuning of the reflection phase of a single band, linearly from $-180°$ to $+180°$, at the operating frequency of 6 GHz, and is employed to design metasurfaces. The zero-phase reflecting metasurface is integrated with the antenna to obtain 4.5 dB more gain than that of the antenna without metasurface. The phase gradient metasurface is employed to tilt the antenna beam, $-44°$ to the normal for RHCP and $+36°$ to the normal for LHCP, resulting in an overall beam steering range of 80°. Thus, the proposed single compact antenna is capable of exhibiting all the above-mentioned functionalities based on electronic switching. This unique feature of the antenna guarantees its significance in cognitive radio applications and wireless communication networks in 5G and beyond.

ACKNOWLEDGEMENT

The authors thank Verdant Telemetry & Antenna Systems Pvt. Ltd., Cochin, Kerala, for their help and support in measuring the parameters of the proposed antenna.

REFERENCES

[1] Mansoul, A., F. Ghanem, M. R. Hamid, E. Salonen, and M. Berg, "Bandwidth reconfigurable antenna with a fixed lower and a variable upper limit," *IET Microwaves, Antennas & Propagation*, Vol. 10, No. 15, 1725–1733, 2016.

[2] Seddiki, M. L., M. Nedil, S. Hadji, and F. Ghanem, "An independently reconfigurable upper and lower band edge of Yagi Uda antenna," *Progress In Electromagnetics Research Letters*, Vol. 96, 1–6, 2021.

[3] Yu, J., W. Jiang, and S. Gong, "Low-RCS beam-steering antenna based on reconfigurable phase gradient metasurface," *IEEE Antennas and Wireless Propagation Letters*, Vol. 18, No. 10, 2016–2020, 2019.

[4] Han, L., G. Cheng, G. Han, R. Ma, and W. Zhang, "Electronically beam-steering antenna with active frequency-selective surface," *IEEE Antennas and Wireless Propagation Letters*, Vol. 18, No. 1, 108–112, Jan. 2019.

[5] Rasool, M., A. Khan, F. Bhatti, B. Ijaz, and A. Iftikhar, "A compact circular loop inspired frequency and bandwidth reconfigurable antenna for 4G, 5G, and X-band applications," *Radioengineering*, Vol. 29, No. 3, 471–478, 2020.

[6] Qin, P.-Y., F. Wei, and Y. J. Guo, "A wideband-to-narrowband tunable antenna using a reconfigurable filter," *IEEE Transactions on Antennas and Propagation*, Vol. 63, No. 5, 2282–2285, May 2015.

[7] Le, T. T. and T.-Y. Yun, "A quad-band dual-sense circularly-polarized square-ring antenna for multi-functional wireless applications," *IEEE Access*, Vol. 7, 149 634–149 640, 2019.

[8] Qin, P.-Y., A. R. Weily, Y. J. Guo, and C.-H. Liang, "Polarization reconfigurable U-slot patch antenna," *IEEE Transactions on Antennas and Propagation*, Vol. 58, No. 10, 3383–3388, Oct. 2010.

[9] Kandasamy, K., B. Majumder, J. Mukherjee, and K. P. Ray, "Dual-band circularly polarized split ring resonators loaded square slot antenna," *IEEE Transactions on Antennas and Propagation*, Vol. 64, No. 8, 3640–3645, Aug. 2016.

[10] Kandasamy, K., B. Majumder, J. Mukherjee, and K. P. Ray, "Beam-tilted and wide beam antennas using hybrid electromagnetic band gap structures," in *2015 European Microwave Conference (EuMC)*, 458–461, Paris, France, 2015.

[11] Cao, Y. F. and X. Y. Zhang, "A wideband beam-steerable slot antenna using artificial magnetic conductors with simple structure," *IEEE Transactions on Antennas and Propagation*, Vol. 66, No. 4, 1685–1694, Apr. 2018.

[12] Ji, L.-Y., Z.-Y. Zhang, and N.-W. Liu, "A two-dimensional beam-steering partially reflective surface (PRS) antenna using a reconfigurable FSS structure," *IEEE Antennas and Wireless Propagation Letters*, Vol. 18, No. 6, 1076–1080, Jun. 2019.

[13] Alqurashi, K. Y., J. R. Kelly, Z. Wang, C. Crean, R. Mittra, M. Khalily, and Y. Gao, "Liquid metal bandwidth-reconfigurable antenna," *IEEE Antennas and Wireless Propagation Letters*, Vol. 19, No. 1, 218–222, Jan. 2020.

[14] Naqvi, A. H. and S. Lim, "A beam-steering antenna with a fluidically programmable metasurface," *IEEE Transactions on Antennas and Propagation*, Vol. 67, No. 6, 3704–3711, Jun. 2019.

[15] Tharehalli Rajanna, P. K., K. Rudramuni, and K. Kandasamy, "Compact triband circularly polarized planar slot antenna loaded with split ring resonators," *International Journal of RF and Microwave Computer-Aided Engineering*, Vol. 29, No. 12, e21953, 2019.

[16] Jacob, N., M. Kulkarni, et al., "Omega shaped complementary split ring resonator loaded bandwidth reconfigurable antenna for cognitive radio applications," *Procedia Computer Science*, Vol. 171, 1279–1285, 2020.

[17] Saha, C. and J. Y. Siddiqui, "Theoretical model for estimation of resonance frequency of rotational circular split-ring resonators," *Electromagnetics*, Vol. 32, No. 6, 345–355, Aug. 2012.

[18] Baena, J. D., J. Bonache, F. Martin, R. M. Sillero, F. Falcone, T. Lopetegi, M. A. G. Laso, J. Garcia-Garcia, I. Gil, M. F. Portillo, and M. Sorolla, "Equivalent-circuit models for split-ring resonators and complementary split-ring resonators coupled to planar transmission lines," *IEEE Transactions on Microwave Theory and Techniques*, Vol. 53, No. 4, 1451–1461, Apr. 2005.

[19] Afridi, A., S. Ullah, I. Ali, S. Khan, and J. A. Flint, "Design and parametric analysis of a dual-band frequency reconfigurable planar dipole using a dual-band artificial ground plane," *IETE Journal of Research*, Vol. 60, No. 1, 3–11, 2014.

[20] Tian, X. and L. Song, "A 2 bit reconfigurable beam-steering antenna array using phase compensation," *Progress In Electromagnetics Research C*, Vol. 126, 63–75, 2022.

[21] Guo, J., Y. Ping, Y. Zhao, Y. Liu, and L. Han, "Design of a full polarization reconfigurable MIMO antenna," *Progress In Electromagnetics Research Letters*, Vol. 110, 73–81, 2023.

[22] Vinod, G. V. and V. V. Khairnar, "A wideband beam steering and beamwidth reconfigurable antenna using coding metasurface," *IEEE Access*, Vol. 12, 97 143–97 153, Jul. 2024.

[23] Paul, P. M., K. Kandasamy, and M. S. Sharawi, "A corner expanded slot antenna loaded with copper strips for dual-band circular polarization characteristics," *Microwave and Optical Technology Letters*, Vol. 62, No. 1, 491–497, Jan. 2020.

[24] Yang, Z.-X., H.-C. Yang, J.-S. Hong, and Y. Li, "Bandwidth enhancement of a polarization-reconfigurable patch antenna with stair-slots on the ground," *IEEE Antennas and Wireless Propagation Letters*, Vol. 13, 579–582, Mar. 2014.

[25] Das, P., K. Mandal, and A. Lalbakhsh, "Beam-steering of microstrip antenna using single-layer FSS based phase-shifting surface," *International Journal of RF and Microwave Computer-Aided Engineering*, Vol. 32, No. 3, e23033, Dec. 2021.

[26] Kaur, K., A. Kumar, and N. Sharma, "Split ring slot loaded compact CPW-fed printed monopole antennas for ultra-wideband applications with band notch characteristics," *Progress In Electromagnetics Research C*, Vol. 110, 39–54, 2021.

[27] Abraray, A., R. A. M. Pereira, K. Kaboutari, and S. Maslovski, "Realization of programmable chessboard mushroom-type metasurface for beamforming applications," in *2023 Photonics & Electromagnetics Research Symposium (PIERS)*, Prague, Czech Republic, July 03-06, 2023.

[28] Yassen, M. T., A. J. Salim, M. R. Hussan, and J. K. Ali, "A compact dual-band dual-polarized antenna based on modified minkowski fractal," *Progress In Electromagnetics Research C*, Vol. 140, 11–19, 2024.

[29] Shen, Z., S. Taravati, and J. Yan, "Digital-coding metamaterials for on-chip beamsteering and reconfigurable millimeter-wave interconnects," *IEEE Access*, Vol. 12, 190 775–190 790, Nov. 2024.

[30] Deshmukh, A. A., H. Mistry, V. A. P. Chavali, A. Viswanathan, and P. Nadkarni, "Reconfigurable designs of sectoral microstrip antennas for single band and tunable circular polarized response," *Progress In Electromagnetics Research B*, Vol. 110, 73–90, 2025.